JOURNAL OF MATERIALS SCIENCE 15 (1980) 2409–2427

Review
Fusion-casting and crystallization of high temperature materials

P. BARDHAN, R. N. McNALLY
Research and Development Laboratories, Corning Glass Works, Corning, New York, USA

Fusion-casting of high temperature materials results in a dense interlocking network of crystals. This method produces the highest strength and most corrosion resistant ceramic materials. Macrosructure and microstructure casting determine the properties of a fusion-cast material. Some of these can be predicted from phase diagrams. Non-equilibrium structures are, however, just as common. Examples of the various cases are discussed for typical industrially important compositions, not only in the oxide systems but in several non-oxide systems.

1. Introduction

1.1. The fusion-casting process

Fusion-casting of refractories came about in the 1920's when Harrison Hood, a Corning scientist, identified stones in a tank glass to be made of a highly refractory alumino–silicate and reasoned that it was so insoluble in the glass that it would make an extremely corrosion resistant refractory lining for a tank. One of his colleagues, Gordon Fulcher, suggested that such a refractory may be formed by electrically melting the material, using the raw material itself as a container. This approach, the effectiveness of which Fulcher demonstrated (using a wooden box to hold the batch in) is the precursor of the modern day skull-melting and electric-arc melting.

Today there are several means of melting highly refractory materials using resistance heating, induction heating, arc heating, arc-image heating, electron-bombardment heating or laser heating. Most of these techniques, however, are used only on the laboratory scale. Commercially, refractory oxides such as Al_2O_3 (m.p. 2043° C), Cr_2O_3 (m.p. 2300° C), ZrO_2 [1], or MgO (m.p. 2825° C) [2] and refractory carbides such as TiC (m.p. 3067° C) [1], ZrC (m.p. 3420° C) [3, 4] or B_4C (m.p. 2450° C) [5–7] are melted in electric arc furnaces.

Raw batch of the desired composition is mixed and then added to the furnace. The unmelted raw batch around the rim of the shell (water-cooled in the large furnace) acts like a container in these vessels. An arc is struck between the electrodes and melting takes place either by resistance heating or arc melting. Materials that have high electrical resistivity can be melted using resistance heating using submerged electrodes. One of the conditions is that the material should not react readily with graphite. In the higher melting materials (> 2000° C), only arc melting is used. In this case, heating is due to the arc as well as to resistance heating. The mode of melting to be used is effected by controlling the length of the arc.

After the melting has been completed, the molten material is cast into a mould. The choice of the mould material depends on the temperature of the liquid. When the melting temperature is extremely high (> 2000° C), as in the case of refractories used in steel plants, graphite moulds are used. The mould is surrounded by annealing sand which is typically alumina. Glass tank refractories with their low melting temperatures are poured into moulds made from sand plates and, as before, surrounded by annealing sand. In special cases where a high chill rate is desired, the material can be cast into water-cooled steel moulds. After a material is cast into a mould, the material may be allowed to solidify completely and cooled to room temperature at a rate sufficiently low that cracking is prevented. In some cases the material is allowed to solidify partially and the mould is stripped. The

0022–2461/80/102409–19 $03.90/0

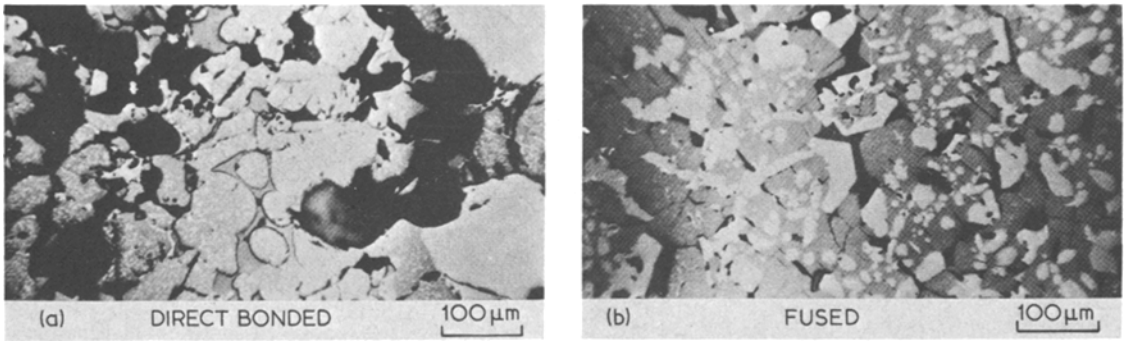

Figure 1 Comparison of the microstructures of fusion-cast magnesia-chrome ore refractory and direct-bonded magnesia-chrome ore refractory.

casting is then allowed to cool down at a controlled rate. After annealing the casting goes through finishing steps such as cutting, grinding and polishing. It is worth noting that fusion cast refractory blocks represent the largest monolithic objects made of ceramic materials.

1.2. Examples of application of fusion-cast materials

Fusion-cast refractories are typified by their dense interlocking network of crystals which will be discussed in greater detail in later sections. This feature, shown in Fig. 1, where the dense fused microstructure is contrasted against the "looser" bonded microstructure, gives these materials significant advantages in corrosion resistance and strength for the same or similar chemistry. (Fused-cast materials contain only closed porosities so that there is no capillary suction of liquid fluxes into the open, interconnected porosity, such as that which occurs in direct bonded materials.) The most common application of fused-cast refractories, therefore, is in their use as a liner material for tanks containing corrosive liquids. They are used as liners in glass tanks and sidewells in metallurgical furnaces. Not only do these materials serve as containers, but also as thermal insulators.

Fusion-cast refractories used in glass tanks include those in the Al_2O_3, Al_2O_3–Cr_2O_3 and Al_2O_3–ZrO_2–SiO_2 systems. The key properties that determine the application are: (1) the rate of dissolution of the refractory; (2) the defect potential of the refractory; and (3) the chemical contamination potential of the refractory. The first merely determines the life of the tank (typically of the order of 3 to 5 years). The second and third affect the quality of the glass. Thus, stones (insoluble refractory crystals in glass), blisters and seeds (such as gas bubbles) and cords (local glass of different index of refraction) and chemical contamination (resulting in, say, change in colour or viscosity of the glass) may arise from use of the refractory. Choice of a given refractory, therefore, must take into account the quality desired in the end product. As examples, Al_2O_3 refractories are used to line glass tanks, Al_2O_3–Cr_2O_3 refractories are used in wool fibre-glass tanks whereas Al_2O_3–ZrO_2–SiO_2 refractories are used as flux blocks for soda-lime glass.

Refractories for steel plant applications have to be resistant to the molten metal as well as to the steel-making slags. In addition, they have to be resistant to thermo-mechanical and thermo-chemical spalling and must not contaminate the steel. The most common fusion-cast refractories for steel-making are made of MgO and chrome ore.

Other applications for fusion cast oxide refractories are those where abrasion resistance is required, e.g., skid rails, grain for grinding and polishing metals, glasses and other ceramics.

Non-oxide fusion-cast refractories were developed when the advent of the space age necessitated the use of thermal shock resistant refractory materials with use temperatures in excess of aluminum oxide (2043° C). Thus, carbide rocket nozzles with excess graphite can be machined from fusion-cast refractory blocks.

1.3. The need for phase diagram studies

To appreciate the microstructures that occur in fusion-cast refractories and to control these microstructures, it is necessary to understand the phase diagram of the system that is being studied. These phase diagrams are not always known for ceramic systems. (For example, although the

MgO–chrome ore system is a commonly employed refractory system, the complexity of the MgO–Cr_2O_3–Al_2O_3–FeO–Fe_2O_3–TiO_2–SiO_2 system deters even the most patient of researchers. White and his co-workers [8–12, 32] in Sheffield have made a significant contribution in this area.) Phase assemblages and their distributions can be controlled through process variables or composition variables. Microstructure control, however, is essential for the optimization of the properties of the material, although macrostructure can, in some cases, play a significant role.

From a knowledge of the phase diagram, the microstructure of a fusion-cast material can be predicted. (As will be shown later, with a knowledge of some fundamental properties, such as the entropy of fusion or dihedral angle between phases, crystal morphology or the geometry of phase distribution can be predicted.) The fact that equilibrium is not always attained often results in unusual microstructures, but even these can be understood from an understanding of crystallization kinetics.

In this review simple systems will be considered, such as: (1) single component systems; (2) binary systems with complete solid solution; (3) eutectic systems with partial solid solubility; and (4) peritectic systems with limited solid solution.

2. Development of structures

2.1. Ingot macro- and microstructure

When a molten material is poured into a mould, freezing proceeds as the latent heat of freezing is removed from the material through the ingot mould. As a result, freezing is initiated first at the mould wall and proceeds directionally from there. Since there is a severe supercooling at the wall, there appears an initial outer *chill zone*. As the heat is extracted perpendicular to the mould wall, *columnar grains* are produced. The rate of heat removal naturally falls (at a parabolic rate) until it is so low that there is sufficient time for free nucleation in the central, unsolidified volume. This results in the central *equiaxed* region being formed. The extent of these regions, however, depends not only on the mould material but on the material that is being cast.

An important feature of a fusion-cast material is its density. To achieve this, it is essential to eliminate all discontinuities or holes in the material. As the material undergoes the liquid-to-solid phase transformation there is a volume contraction and consequently it is not practically possible to eliminate "pipes" that result in a cast ingot. The understanding of the formation of pipes may be helped by consideration of a volume of liquid freezing in a mould. If no heat is lost laterally and heat extraction occurs through the bottom of the mould only, the isothermal surface is a horizontal plane and there is a pipe, the shrinkage associated with the liquid–solid volume contraction which is accounted for by a difference between the original level of the liquid and the final level of the solid. Lateral heat flow, however, cannot really be avoided. As a result, depending on the relative amounts of heat lost in the vertical and horizontal directions, a concave isothermal surface results. This concavity dictates the extent of the pipe. If freezing takes place from the top as well as from the sides and bottom, a totally enclosed pipe is formed.

In addition to shrinkage pipes, the evolution of gases during solidification (and during coating of the superheated liquid prior to solidification) results in small cavities in the body of the refractory, called blow-holes. The dissolution and exsolution of gases from liquids are analogous to the dissolution and precipitation of a second phase in the solid state. Thus, at the high fusion temperatures, gases dissolve in the melt. During freezing, as the temperature drops, the liquid becomes supersaturated with respect to the dissolved gas so that as soon as a critical gas nucleus forms, this "precipitates" out of the liquid. The gas bubbles may coalesce upon being released or be trapped in place as rapid freezing occurs. In some systems, gas evolution is inevitable as is the case in the Fe–O system.

If a composition such as Fe_2O_3 were to be fusion-cast, the refractory would have blow-holes arising from the liberation of oxygen. This can be appreciated from a phase diagram. The Fe_3O_4–Fe_2O_3 phase diagram, determined by Phillips and Muan [13], is shown in Fig. 2. When Fe_2O_3 is heated in air so that equilibrium is maintained with the atmosphere, loss of oxygen starts at a temperature of 1388° C until the conversion to non-stoichiometric magnetite (oxygen-excess) is complete. (Since the three phases, of two solids and a gas, co-exist, the system is univariant. As the pressure is constant, the transformation to magnetite is completed at constant temperature.) In the resulting bi-variant system, oxygen is lost progressively until the melting point is reached. The system once again becomes univariant, with three phases, solid, liquid and gas, and melting

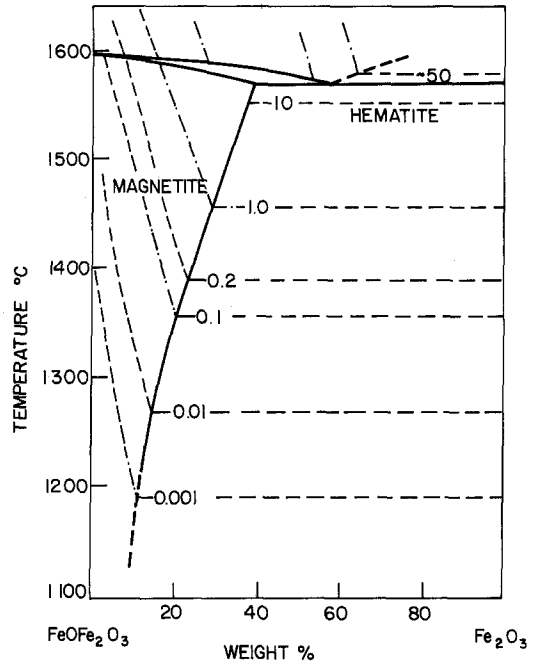

Figure 2 The Fe_3O_4–Fe_2O_3 phase diagram (Phillips and Muan [13]).

proceeds at constant temperature with pick-up of oxygen. When this liquid is cooled, the changes occur in reverse, with oxygen being given off during freezing with formation of magnetite. This cycle of reduction, oxidation and reduction therefore results in the appearance of blow-holes in the cast Fe–O refractory. These blow-holes can sometimes be suppressed, as described by Wilshee and White [14] for the Mg–Fe–O system.

2.2. Pure systems

Pure materials and dilute alloys (or solutions) freeze over a very narrow temperature range. (In the case of pure systems this occurs at a discrete temperature, T_m.) The tendency in this case is to form large, orientated crystals. This feature is seen in a chill casting of pure MgO (98%), a micrograph of which is shown in Fig. 3. Note that voids form between the columnar crystals. The large size of the grains, and the fact that they are orientated, results in low strength and intercrystalline shear at high temperatures, making long term durability (of special importance in glass refractories) a major problem. Fortunately, the crystal size and orientation can be modified by an appropriate choice of additives, as will be demonstrated later. It should also be noted that pure systems are not necessarily desirable because individual grains in these systems have a continuous film of low

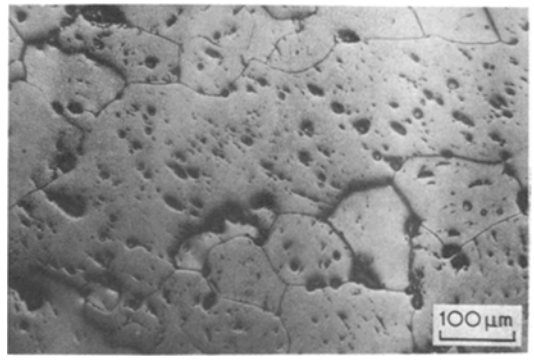

Figure 3 The microstructure of fusion-cast MgO showing the large orientated grains.

melting phases, such as silicates, arising from trace impurities. Such a film leads to a loss in hot strength [15].

2.3. Systems containing complete solid solutions

In the simplest binary system the two components are isomorphous and able to dissolve completely into each other in all proportions. In systems such as MgO–FeO or MgO–NiO, complete solid solution occurs between the two end members at all temperatures if the valence of the transition metal cation is unaffected. As in the case of pure oxides, the chill cast materials have a tendency to form large, columnar crystals, perpendicular to the freezing isotherms. In a similar fashion the low melting impurity phases (generally silicates) surround and coat the crystals. This latter characteristic is the primary reason for avoiding single phase fused-cast materials. White [8–12] has shown in a series of papers that the presence of a second intergranular phase (for example, $MgCr_2O_4$ in MgO) will cause an increase in the dihedral angle so that the low melting silicates can be isolated into pockets. This is an important consideration in the design of refractory products.

2.4. Eutectic microstructures

The Al_2O_3–ZrO_2 binary is a simple eutectic system which has recently been redetermined by Manfredo *et al.* [16]. There is little, if any, solid solubility of one end member in the other. The change in microstructure going from the hypo-eutectic to the hypereutectic compositions is shown in Fig. 4. At the eutectic composition, the microstructure is a composite of rods of ZrO_2 suspended in a corundum matrix.

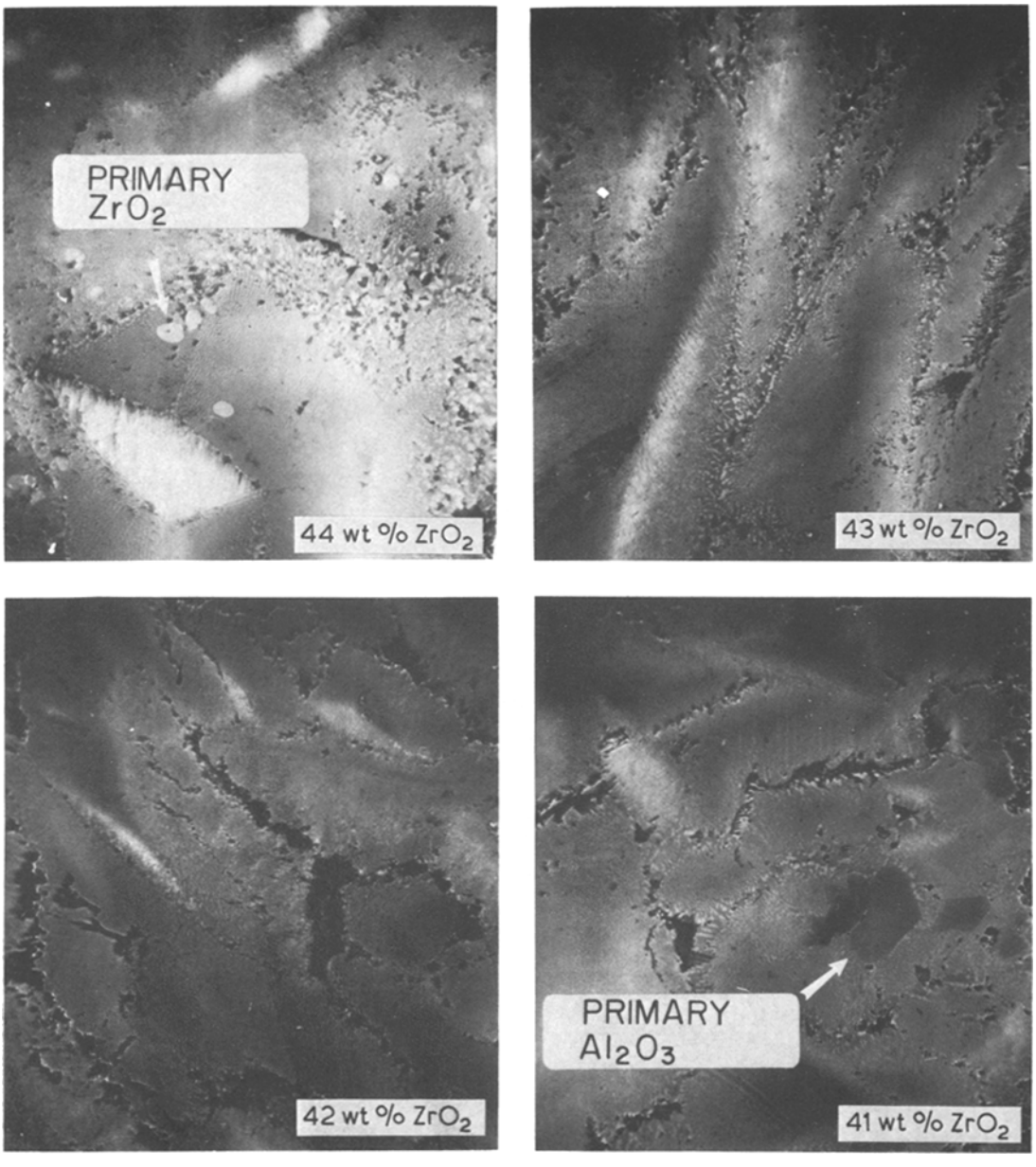

Figure 4 The microstructure of hypoeutectic, eutectic and hypereutectic Al_2O_3–ZrO_2 compositions.

Away from the eutectic, crystals of the primary phase, α-corundum or zirconia, occur with their characteristic morphologies. Thus, ZrO_2 crystals appear as blebs whereas Al_2O_3 crystals are euhedral. Jackson and Hunt [17, 18] have developed a theory according to which the roughness of the solid–liquid interface (or an atomic scale) governs the growth morphology. That is, the entropy of the phase change, which is small for rough surfaces and large for smooth surfaces, determines the morphology of the phases. Uhlmann [19] has also suggested that crystals with entropy of melting between $2R$ and $4R$ can develop planar interfaces or be facetted and where ΔS_f is greater than $4R$, crystals exhibit facetted growth. The oxides described here have entropies of fusion between $2R$ and $4R$; thus MgO with $\Delta S_f \sim 3R$ shows non-facetted growth, ZrO_2 with $\Delta S_f \sim 3.45R$ shows the bleb-like morphology whereas Al_2O_3 with $\Delta S_f \sim 5.5R$ exhibits facetting.

Eutectic materials are of more than passing interest to materials scientists. They are, as pointed

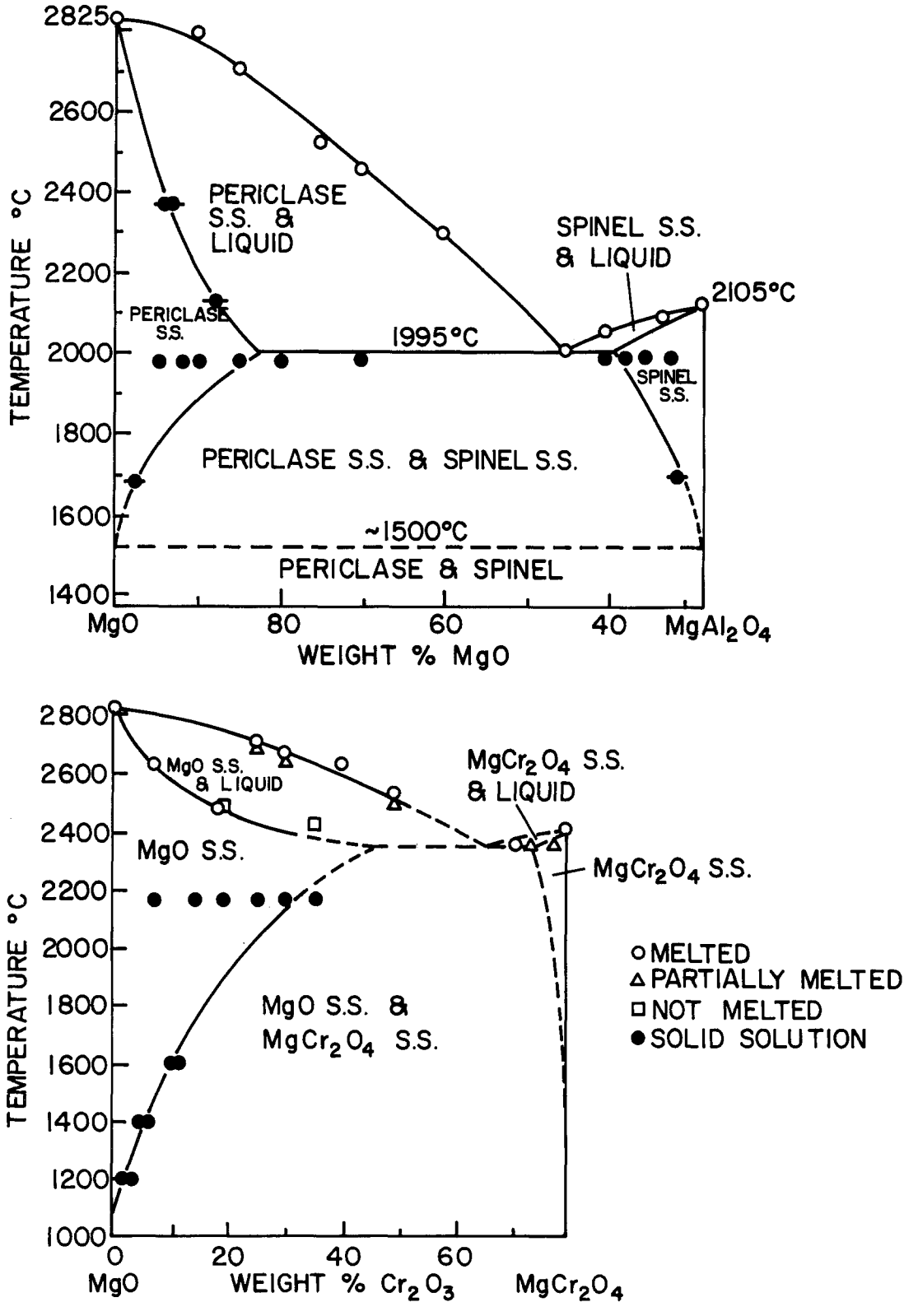

Figure 5 Equilibrium phase diagrams in the $MgO–MgAl_2O_4$ system and the $MgO–MgCr_2O_4$ system.

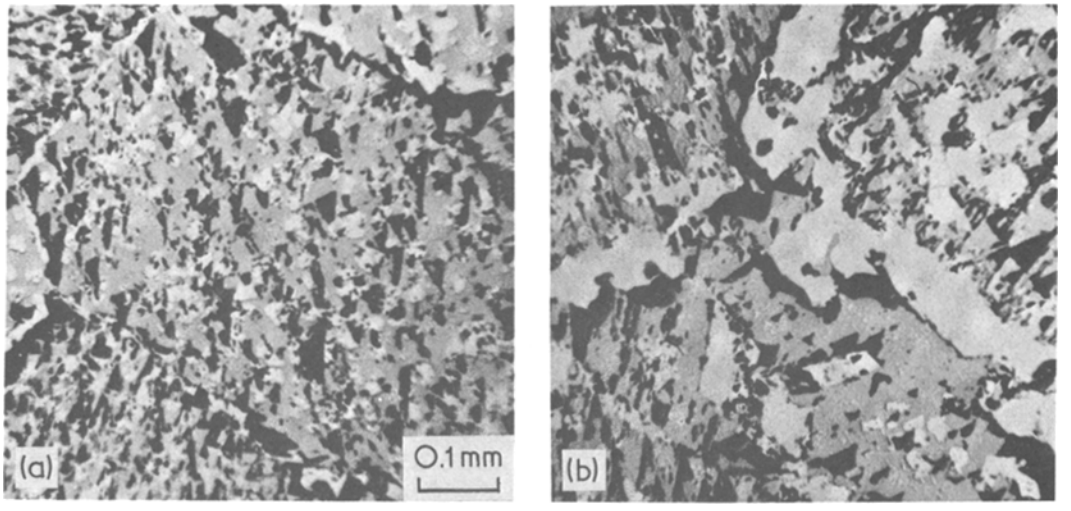

Figure 6 Polished sections of quenched specimens showing periclase solid solution with precipitated picrochromite solid solution. (a) 55 wt% MgO–45 wt% Cr_2O_3. (b) 50 wt% MgO–50 wt% Cr_2O_3. (b) also contains intergranular picrochromate solid solution.

out earlier, natural composites wherein one phase with a lamellar morphology or rod-like morphology lies embedded in a matrix of the second (greater volume fraction) phase. The material then has all the features of fibre-reinforced materials. Indeed, this has been the impetus for research in unidirectionally solidified ceramics [20, 26].

2.5. Eutectic systems with partial (limited) solid solubility

Fig. 5 shows the phase diagrams of two systems $MgO–MgAl_2O_4$ and $MgO–MgCr_2O_4$ determined by McNally *et al.* [21, 22]. Note that in the $MgO–MgAl_2O_3$ system, less than 20 wt% Al_2O_3 (i.e., 28.6% spinel) is in solution at the eutectic temperature. In the $MgO–MgCr_2O_4$ system, however, more than 40 wt% Cr_2O_3 (i.e., 52.5% spinel) is in solution in the MgO. This is because of the larger difference in the size of Al^{+3} and Mg^{2+} ions. As a result, the periclase grains in the fused-cast microstructure of the two systems appear to be affected in a different manner. In the $MgO–MgAl_2O_4$ system, although a hypoeutectic composition may be slowly cooled, there is little evidence of exsolved spinel within the rounded periclase grains. Upon aging, the dissolved spinel will eventually precipitate out within the MgO. (This occurs because of the sloping solvus curve; that is, with decreasing temperature the periclase is supersaturated with respect to the spinel dissolved at a higher temperature. The temperature is sufficiently high to result in exsolution of spinel.) However, in the $MgO–MgCr_2O_4$ system, as seen from Fig. 6, in addition to the intergranular spinel (picrochromite) the slow-cooled material shows exsolved spinel. This occurs because the supersaturation of the spinel (the driving force for the precipitation raction) is much greater in the $MgO–MgCr_2O_4$ system than in the $MgO–MgAl_2O_4$ system. Indeed, to suppress the exsolved spinel one would have to solidify and cool the compositions in this system very rapidly.

2.6. Microstructure in peritectic systems

In the peritectic reaction, the liquid L_p reacts with the solid α_p to form the new phase β_p:

$$L_p^{(l)} + \alpha_p^{(s)} \underset{\text{heating}}{\overset{\text{cooling}}{\rightleftharpoons}} \beta_p^{(s)}.$$

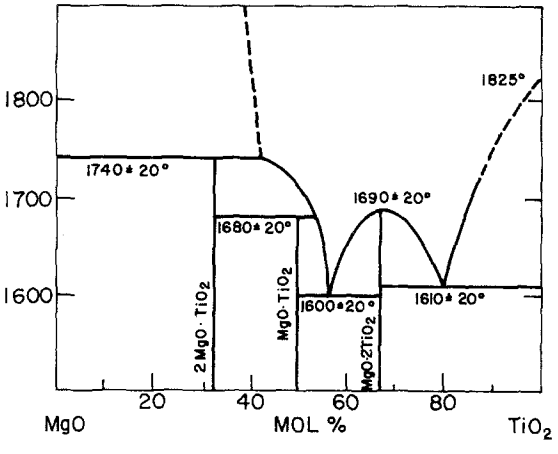

Figure 7 The equilibrium phase diagram in the $MgO–TiO_2$ system.

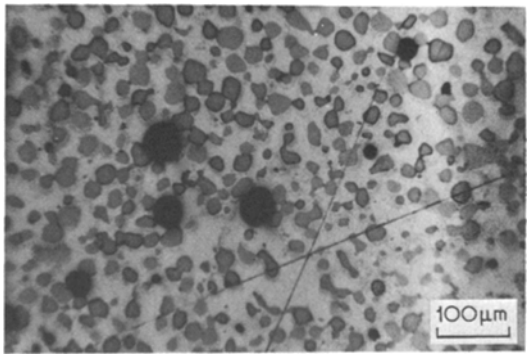

Figure 8 Polished section of 48 wt% MgO–52 wt% TiO_2 showing the coring resulting from the incomplete peritetic reaction.

This results in a layer of β_p at the interface between L_p and α_p. The formation of this initial layer of β_p tends to reduce the rate of further reaction. The layer of β_p tends to vary in composition all the way from the ideal peritectic composition, β_p, to the composition of the initial liquid, β_f. Therefore, the β phase is cored and lies around α_p. Unless the solidification and the subsequent cooling rate is very slow, non-equilibrium microstructures are characteristic of such systems.

Fig. 7 shows the equilibrium phase diagram for the MgO–TiO_2 system [23]. The effect of the incomplete peritectic reaction on the microstructure of the 48 wt% MgO–52 wt% TiO_2 is shown in Fig. 8 where the original orthotitanate spinel crystals (2 MgO · TiO_2) are seen to have a layer of the MgO · TiO_2 reaction product. The peritectic liquid is also seen as the matrix in the micrograph.

3. Microstructures in fusion-cast non-oxide systems

3.1. Eutectic microstructures

Consider the B–C system. The B_4C–C section of the phase diagram has a eutectic at 2375° C [5]. The change in the microstructure from the eutectic (at 45.6 wt% B–54.4 wt% C) to a hypereutectic composition, with increasing C, is shown in Fig. 9. Large primary graphite flakes appear surrounded by the B_4C–C eutectic. These flakes get coarser with increasing graphite content. The B_4C–C system is of interest because it is an extremely light-weight material. The density of B_4C is 2.51 g cm^{-3} and that of graphite is 2.25 g cm^{-3}. The material cannot, however, be easily fusion-cast. For ease of melting, therefore, Si^0 is added, resulting in a body containing SiC.

The control over the microstructure desired and the flexibility that one has increases if, instead of a binary system, a ternary system is chosen. Consider the ternary Zr–B–C system. The calculated phase diagram, showing the compatibility triangles and the liquidus projections are shown in Fig. 10 [25]. Examples of the changes in the microstructure are

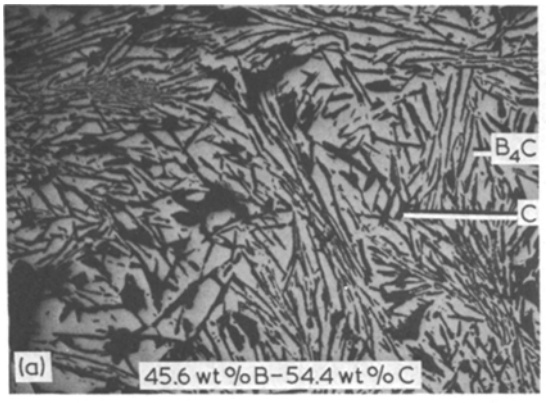

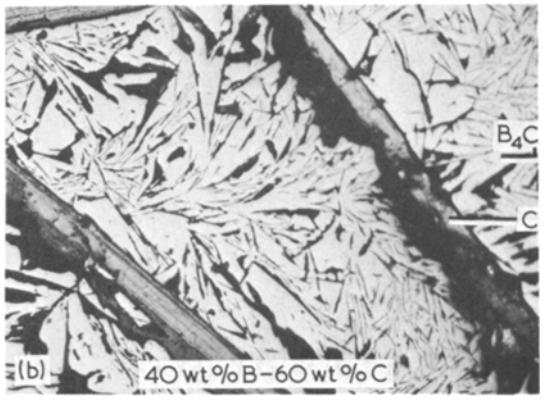

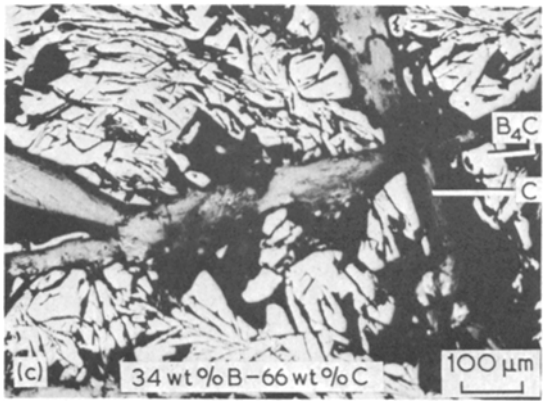

Figure 9 Microstructures developed in eutectic B_4C–C (45.6 wt% B–54.4 wt% C) and hypereutectic compositions. Note the coarsening of the graphite plates with increasing carbon content.

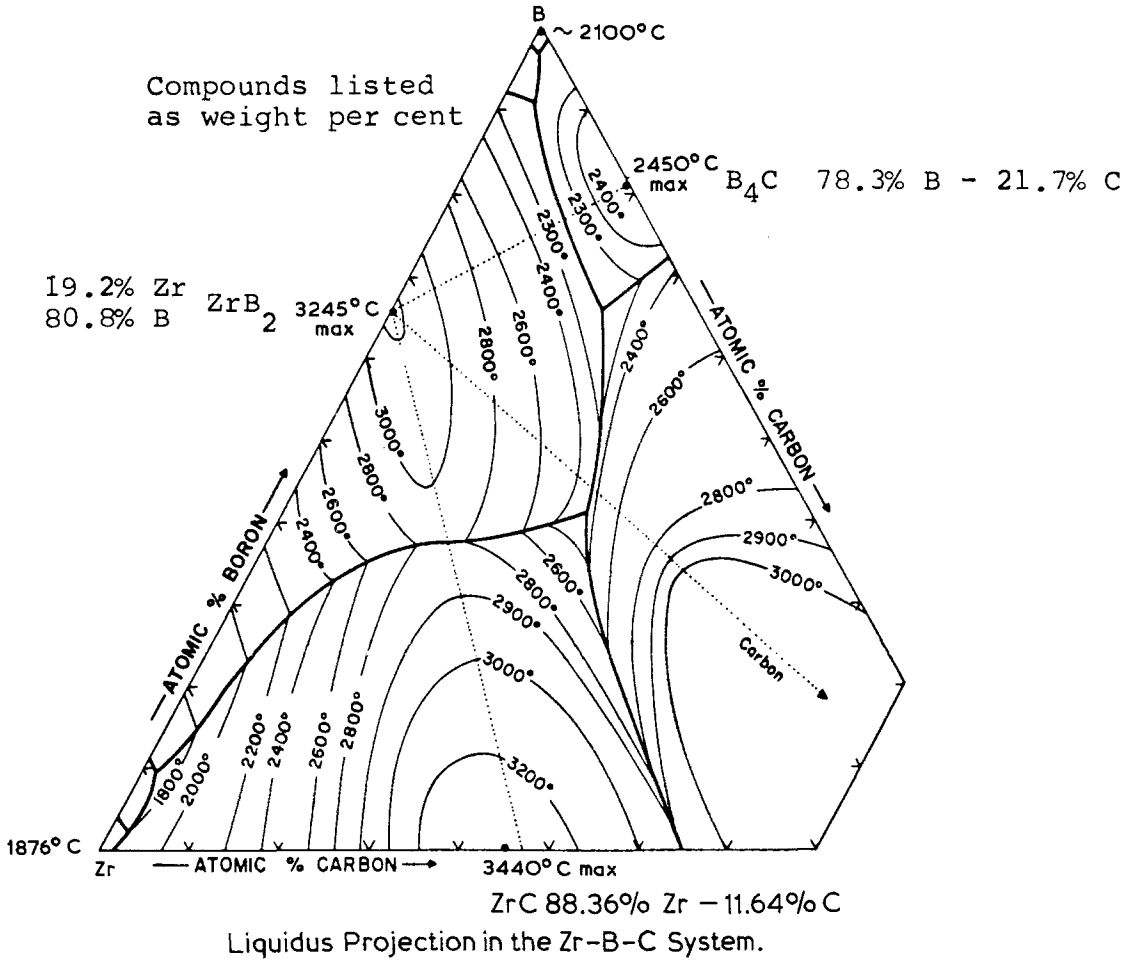

Figure 10 Calculated phase diagram showing liquidus projections and compatibility triangles in the Zr–B–C system [25].

shown in Fig. 11. These represent compositions in different compatibility fields, for example, B_4C–ZrB_2–C and ZrB_2–ZrC–C. The properties of the resulting bodies are naturally quite different and give rise to different casting problems [24].

3.2. Peritectic microstructure

Carbide–graphite systems that melt incongruently on cooling first have graphite crystallizing out; then the primary graphite reacts with the metal-rich liquid to form the carbides. As is to be expected, these reactions are often not completed and this results in the non-equilibrium phase assemblages. In the Cr–C system the intermediate compounds such as Cr_3C_2, Cr_7C_3 and $Cr_{23}C_6$ melt incongruently. Consequently a peritectic composition such as Cr–13 wt % C shows not only Cr_7C_3 and Cr_7C_3 but the unreacted graphite as well. An example is shown in Fig. 12. Similar non-equilibrium phase assemblages result in the other group VIB–graphite systems. Of the carbides, this is one of the more conveniently melted and cast bodies. It will find application where moderate refractoriness is desired (liquidus ~ 1900° C), with excellent thermal shock resistance and good oxidation resistance up to 1550° C.

3.3. Combinations of eutectic and peritectic systems

The relation between the microstructure and the type of solidification, peritectic or eutectic, is shown in Fig. 12. The eutectic microstructure, for example, Ti–C, being characterized by the presence of fine graphite platelets in the intergranular eutectic in addition to the coarser primary graphite (the composition shown is a hypereutectic). This is to be contrasted with the peritectic microstructure, for example, Cr–C, where primary

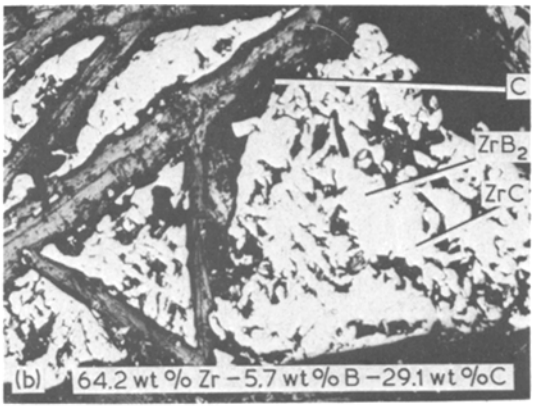

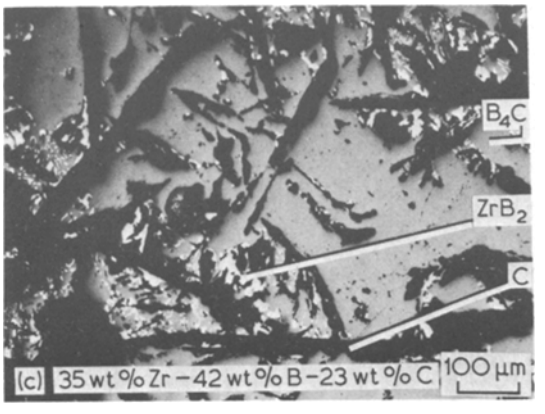

Figure 11 Fusion-cast microstructures in different compatibility fields in the Zr–B–C system.

graphite flakes form and are surrounded by the carbide reaction produce with no included fine graphite. This suggests that a further control over microstructure can be exercised by a combination of the two systems.

The result of such a combination is shown in Fig. 13. The effect of Cr addition can be summarized as follows. Below 4.6 wt % retained Cr, only two phases exist, a (Ti, Cr)C solid solution and graphite. At, and above 4.6 wt % Cr, a third (Ti, Cr)C phase which contains a higher amount of Cr is detected. When Cr is increased to 25 wt % a fourth phase, Cr_3C_2, appears. A more significant change that occurs is in the distribution of the graphite phase. As the Cr content increases, the amount of intergranular graphite decreases. At 18 wt % Cr, the graphite occurs primarily as large blades, and only a very small amount of intergranular (eutectic) graphite can be detected. Such modifications are important for fine control over properties. For example, the addition of Cr, through this type of microstructural change greatly enhances the oxidation resistance of the TiC–C body. Typically, TiC–C refractories oxidize rapidly at temperatures between 500° C and 700° C where a loose, non-adhering anatase oxide forms. At 1000° C, a denser and more tenacious rutile film forms, resulting in a sharp decrease in the oxidation rate. By 1500° C, however, the rate of oxidation again increases. It is in this range that the addition of Cr retards the oxidation rate.

4. Problems in fusion-casting (and some solutions)

In this section, some practical problems unique to the fusion-casting process are considered. Where applicable, solutions are described.

Not all compositions are readily manufacturable. In order to render a desired *microstructure* manufacturable it will become apparent that it is necessary to use knowledge of materials, phase diagrams and solidification. This was found to be the case with B_4C–C, where Si^0 was intentionally added to obtain dense, crack-free castings. This is one example of the use of an unconventional additive. Another example is given below.

4.1. The use of a glass phase

Because of the polymorphic transition of ZrO_2, the material cannot be fusion-cast without allowing for stress relief. Thus a glass phase is used in order to make high ZrO_2 compositions manufacturable.

Zirconia–alumina–silica fusion-cast refractories have been used commercially with ZrO_2 contents generally between 30 and 42 wt %. These refractories are a mixture of interlocking crystalline phases (corrundum and zirconia) and an interstitial glass phase. These refractories perform well in con-

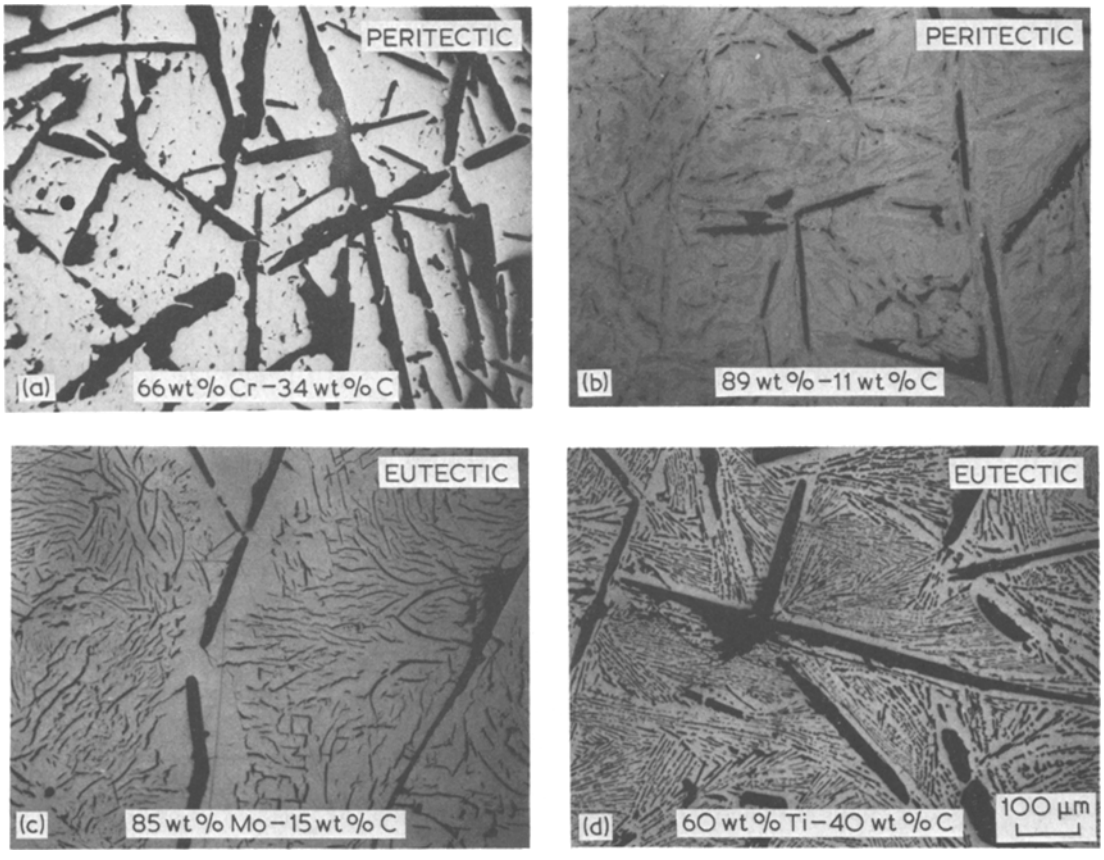

Figure 12 Polished sections in metal–carbon systems showing the different types of microstructures that result depending on the phase diagram.

tact with many glasses melted at 1500° C or lower; they have been found to more readily react with many glasses melted at higher temperatures. The greater reaction results in loose crystalline particles of the refractory (called stones) that float off into the glass melt. These stones cause defects in the finished glass article. Some molten glasses with higher melting temperatures cause high rates of corrosive wear on the 30 to 40 wt % refractories.

In a tank producing sodium aluminosilicate glass, the commercially available 30 to 40 wt % ZrO_2 fusion-cast refractories form an undesirable surface layer on the refractory when cooled upon shutdown for repairs. When the tank is reheated, the surface layers of these refractories in contact with molten glass undergo exfoliation producing many stones which affect the glass quality.

The development of many new glass compositions requiring higher melting temperatures of between 1550 and 1850° C or greater, resulted in a need for improved refractories that are not subject to high stoning rates and excessive corrosive wear during the full useful life of the refractories.

Our approach [27] provides a ZrO_2–Al_2O_3–SiO_2 fusion-cast refractory having high ZrO_2 content that can be readily manufactured on a commercial basis as glass blocks large enough for lining glass tanks. These fusion-cast high ZrO_2 refractories can be cast crack-free, or with minor cracks well within the industry specifications. A good refractory was found to be: 68 to 82.5 wt % ZrO_2, 10 to 22 wt % (preferably at least 15%) SiO_2, 0.5 to 2.5 wt % Na_2O, not more than 1 wt % (desirably less than 0.4%) $Fe_2O_3 + TiO_2$, and Al_2O_3 in an amount such that the ratio Al_2O_3/SiO_2 is between 0.3 and 0.65. The latter ratio assures a very high recovery rate of essentially crack-free cast products and restricts the amount of corundum and/or mullite crystals to no more than between 25 and 30 vol % of the total refractory minus the volume of ZrO_2 crystals.

The test data in sodium aluminosilicate glass is shown in Table I.

These high ZrO_2 compositions within the above range consist primarily of crystalline zirconia with a siliceous glass phase as a matrix between the

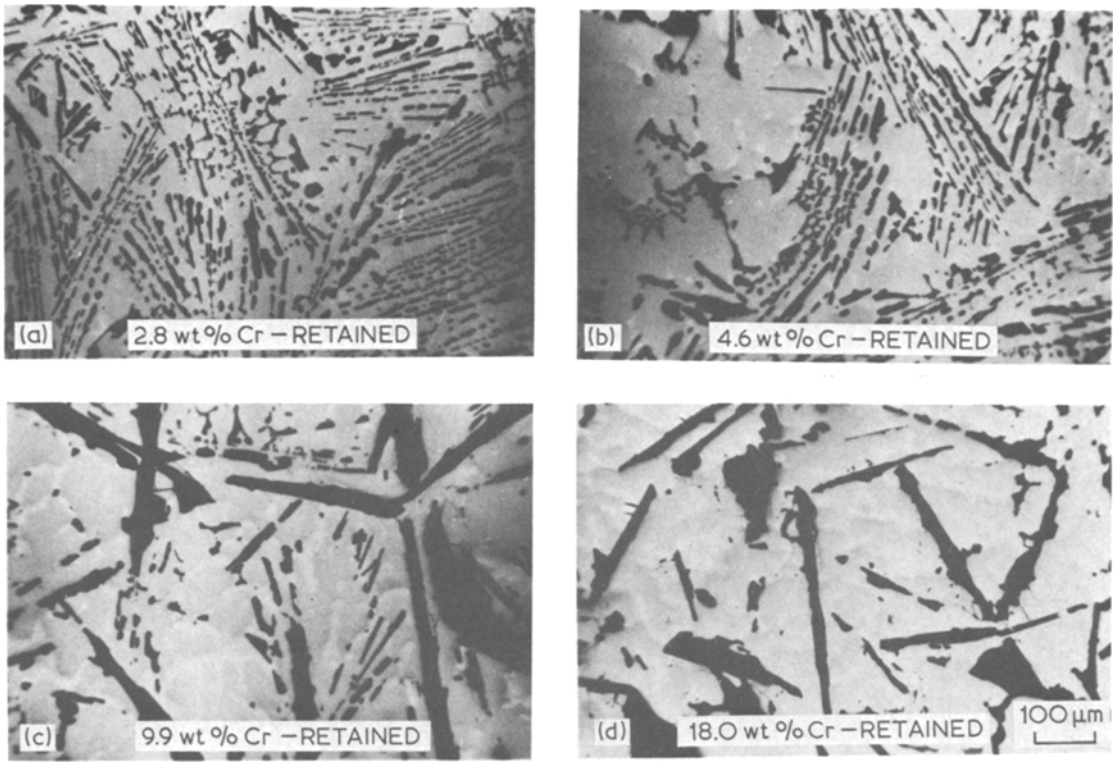

Figure 13 The effect of Cr addition on the dispersion of graphite in the TiC–C system.

zirconia crystals. In some cases, the refractory may also contain, within the glass phase matrix, minor amounts of mullite crystals and/or corundum crystals, the largest total amount of both being about 40 to 50 vol% by volume of the total volume of glass phase. Volume proportions of mullite and/or corundum crystals greater than 50% appear to be related to the cracking of high ZrO_2 fusion-cast refractories.

4.2. The use of a second crystalline phase

The fusion and casting of a commercial grade alumina oxide (> 99% pure) resulted in an orientated structure with a pattern of elongated columnar crystals mutually orientated and essentially perpendicular to the isotherm of the casting. This is shown in Fig. 14. The coarse grained structure had poor thermal shock resistance (lasting only 1 cycle in the test described below) because of the ease of fracture between the mutually orientated crystals. It was found that by adding a second component of CaO a structure comprising of fine interlocking crystals of corundum and alkaline earth metal hexaluminate ($CaO \cdot 6Al_2O_3$) was obtained [28]. This new structure resulted in an increase in thermal shock resistance as shown in Table II. The thermal shock test consists of a $1 \times 1 \times 3$ inch^3 sample which is placed in a gas oxygen furnace at 1650° C. The sample is held at this temperature for 10 minutes and then pulled out of the furnace and cooled to

TABLE I Property data

Melt Number	ZrO_2	Al_2O_3	SiO_2	Na_2O	Al_2O_3–SiO_2	Crack index	Stoning potential	Corrosion cut (mm)	
								Melt line	Mid-point
1369	76.2	1.5	20.6	1.4	0.22	1 –	0.5	0.65	0.16
851	71.1	10.4	16.7	1.5	0.62	1 –	0.5	0.52	0.18
1407	69.6	14.2	14.7	1.4	0.97	2	0.5–1	0.54	0.12
1400	56.0	22.9	19.0	1.9	1.21	4 +	1.5–2	Cut off	
833	58.2	23.0	17.0	1.6	1.36	3 +	2.5–3	Cut off	

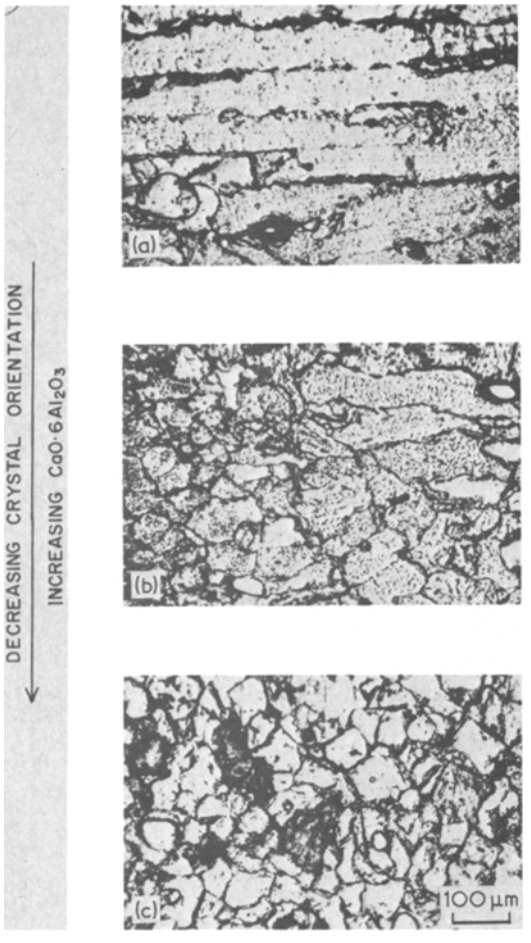

Figure 14 The effect on crystal orientation, in fusion-cast Al_2O_3, of a second phase ($CaO \cdot 6Al_2O_3$).

room temperature. This constitutes one cycle. The sample is examined for cracking and spalling. The test is continued until the specimen is spalled. The formation of the $CaO \cdot 6Al_2O_3$ phase does not have an adverse effect on the thermal shock of Al_2O_3 because both corundum and calcium hexaluminate phases have the same coefficient of thermal expansion at 1000° C of 83×10^{-7}.

The addition of the metal fluoride increased both the modulus of rupture of the castings and the manufacturability. The average room temperature modulus of rupture of fusion-cast, essentially-pure aluminium oxide which had grain orientation was $1.4\,MN\,m^{-2}$. With the addition of the alkaline-earth metal oxide, the modulus of rupture increased to an average of $2.6\,MN\,m^{-2}$. The combined alkaline-earth metal hexaluminate and metal halide resulted in an average modulus of rupture of $4.8\,MN\,m^{-2}$.

TABLE II Variation in thermal shock resistance

Mole per cent by analysis	Thermal shock cycle
98.79% Al_2O_3–1.21% CaO	13
97.67% Al_2O_3–1.44% CaO–0.89% F_2	11
96.42% Al_2O_3–3.58% CaO	22
97.36% Al_2O_3–1.76% CaO–0.88% F_2	23

4.3. The elimination of a second phase

A second phase does not always enhance the properties of a fusion-cast refractory. In such cases, the easiest route is *not* always the elimination of the constituents that result in the second phase. Thus, in fusion-cast MgO–spinel refractories, the spinel is required not only for strength in the refractory body but it also acts as a mineralizer which renders the material manufacturable. But it does give rise to other problems.

When the R^{3+} ions, such as Cr^{3+} and Al^{3+} ions, go into the MgO lattice in solid solution, defects arise on the cation sub-lattice. Consequently, the structure is unstable, and, depending on the temperature, these ions will either go into the solution or precipitate out.

Fig. 15 is a schematic comparison of the MgO with R^{3+} in solid solution and $R^{3+} + R^{1+}$ containing MgO solid solution lattice. For example, when Li^{1+} is added along with R^{3+} to MgO, the cation defects are significantly decreased [29]. This results in a more stable periclase solid solution. Consequently when Li^{1+} is added to MgO–R_2O_3 system, e.g. MgO–chrome ore system, the spinel phase is drastically decreased and very little precipitation of the spinel phase occurs during cooling.

Fig. 16 shows the progressive change in the microstructure of fusion-cast MgO–chrome ore refractory as Li_2O is added to the refractory [29]. (Some Li_2O does dissolve in the silicate phase. This reduces the MgO–MgO bonding in the system and is circumvented by using better grade starting batch materials, with a lower SiO_2 content.)

Two significant effects of the Li_2O addition, on properties, are to be noted: firstly, as a result of the phase-stability over a cycling temperature range (from 1250° C to 1650° C) the refractories do not grow as readily after undergoing cyclic heat treatment; and secondly, the hydration resistance of the MgO–chrome ore–Li_2O is greatly increased. There are two possible reasons for the increased hydration resistance. The Li_2O, by decreasing the defect concentration, decreases

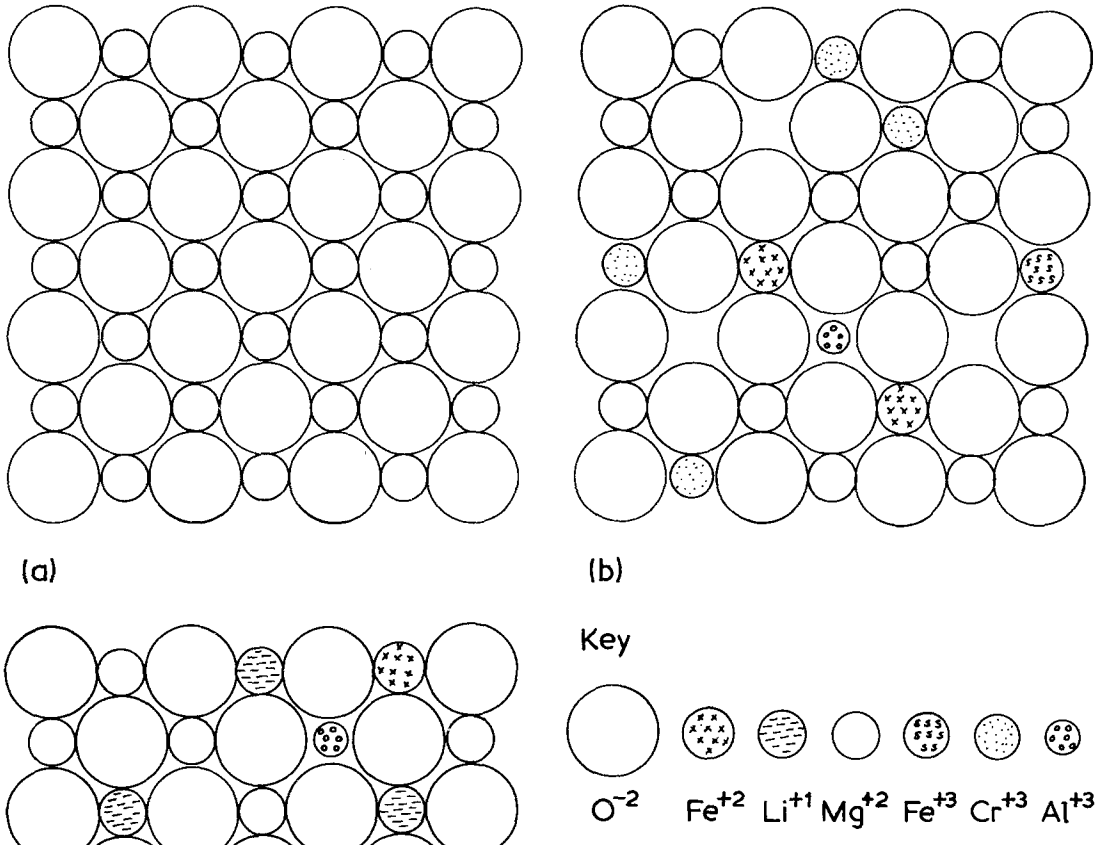

Figure 15 Schematic representations of (a) periclase lattice, (b) periclase solid-solution lattice and (c) lithium-containing periclase solid-solution lattice.

the internal stresses and thereby retards hydration. Alternatively, it is possible that the incorporation of the more hydration-resistant spinel phase results in solid solution that is intrinsically more chemically durable.

4.4. Intergranular versus intragranular second phase

Consider the $MgO–TiO_2$ system. Two types of spinels can form in this system depending on the state of oxidation of the cation. Thus, when the Ti ion is present in the 3 + state, $MgO \cdot Ti_2O_3$ spinel results. This is readily soluble in the periclase at high temperatures but exsolves as the refractory cools down to room temperature. Consequently these Ti–spinels occur primarily as intragranular precipitated spinel in individual periclase grains. This is shown in Fig. 17. If, however, the same composition is melted under more oxidizing conditions, the Ti ions occur in the 4 + state (there is less than 1 to 1.5% Ti^{3+} in this material), and the incongruently melting Mg_2TiO_4 spinel that results occurs only as an intergranular phase. This rearrangement of phases causes a significant change in the properties. As an example, the Ti^{3+} refractory body is unstable and converts to Ti^{4+} when heated in air at high temperatures. Growth (due to phase changes) in such a refractory can cause a catastrophic degradation of the refractory body.

4.5. A problem that remains

In addition to considerations of microstructures, the macrostructure of the castings must also be considered. Thus, a composition may not be easily manufacturable if the casting has (even fine)

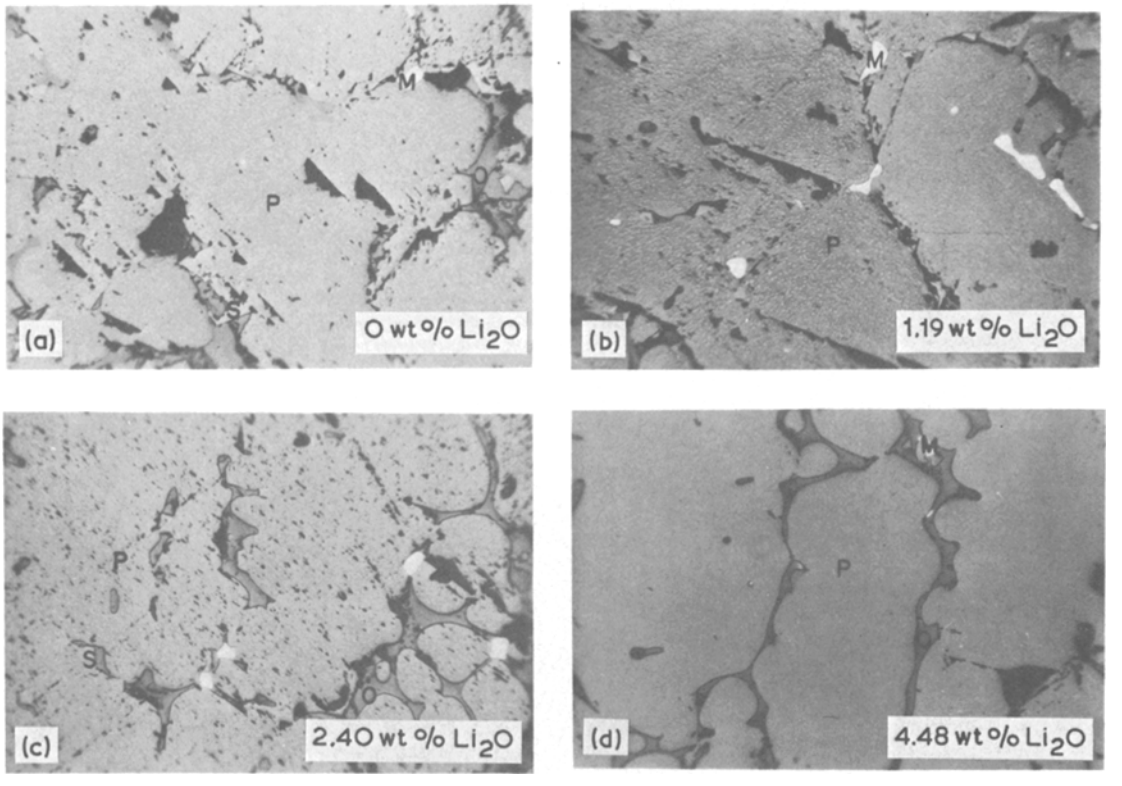

Figure 16 The progressive change in microstructure of MgO–chrome ore refactory with the addition of Li_2O.

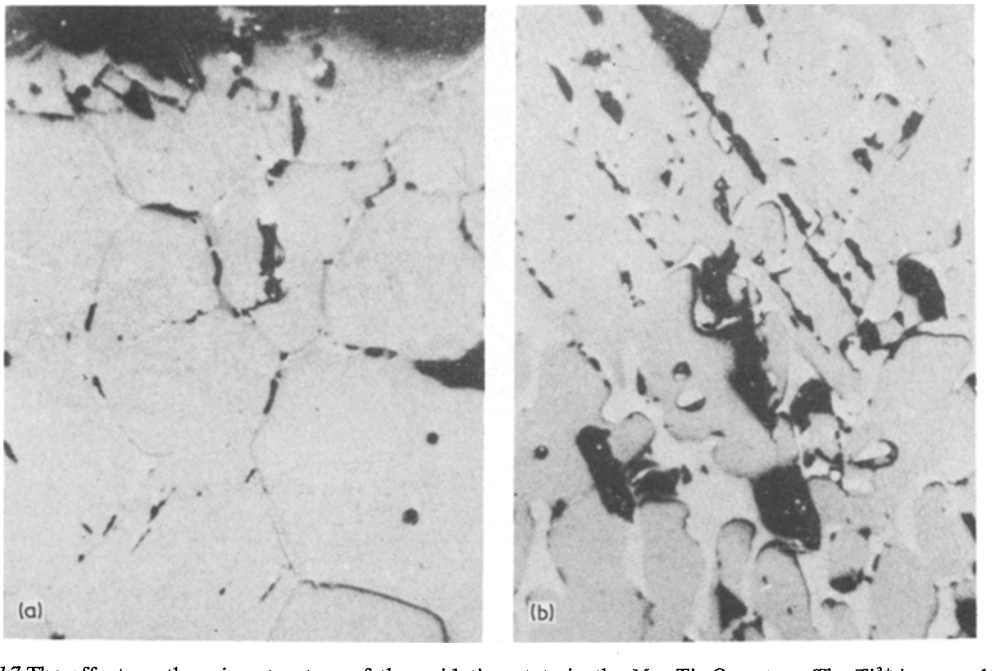

Figure 17 The effect on the microstructure of the oxidation state in the Mg–Ti–O system. The Ti^{3+} ions result in the $MgO \cdot Ti_2O_3$ spinel which goes into solution in the MgO and exsolves as the intragranular phase. With Ti^{4+} only the intergranular orthotitanate spinel results.

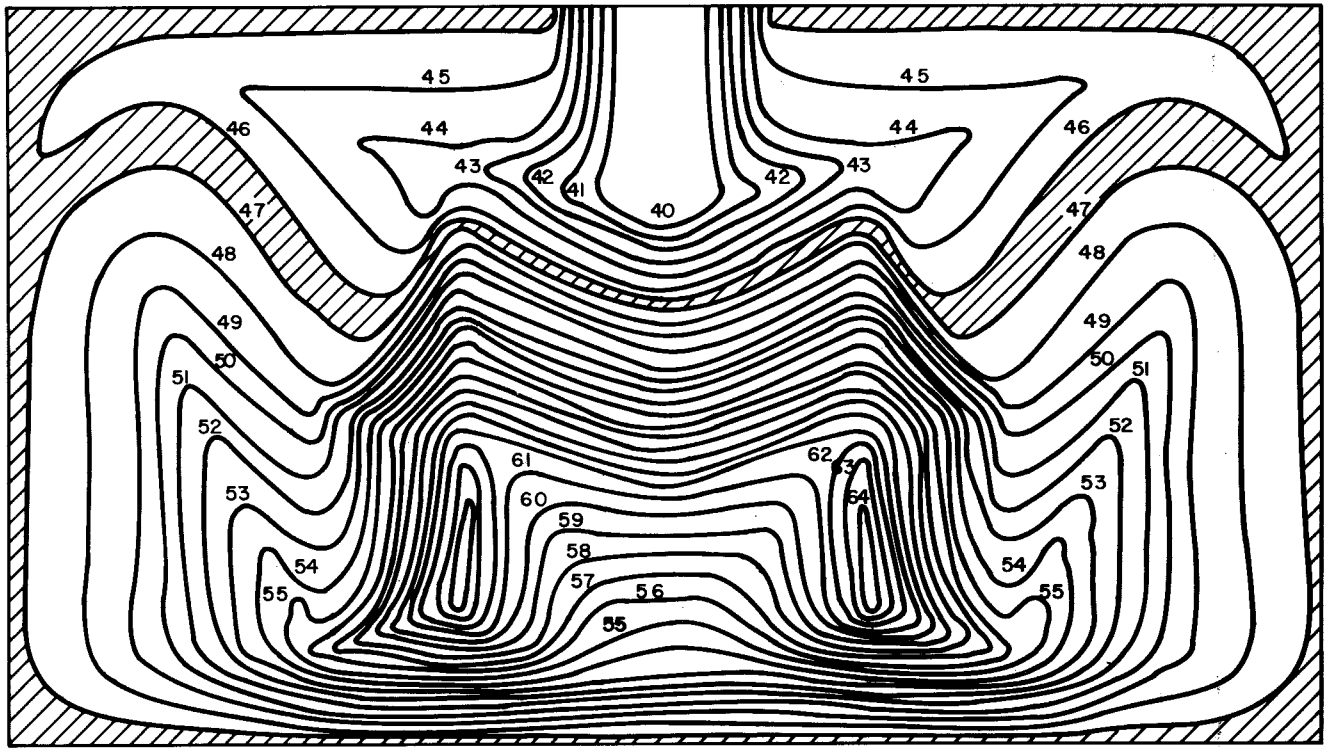

Figure 18 Density-caused segregation in Al_2O_3–ZrO_2–SiO_2 fusion-cast refactories. The contours reflect the weight per cent ZrO_2 in the block.

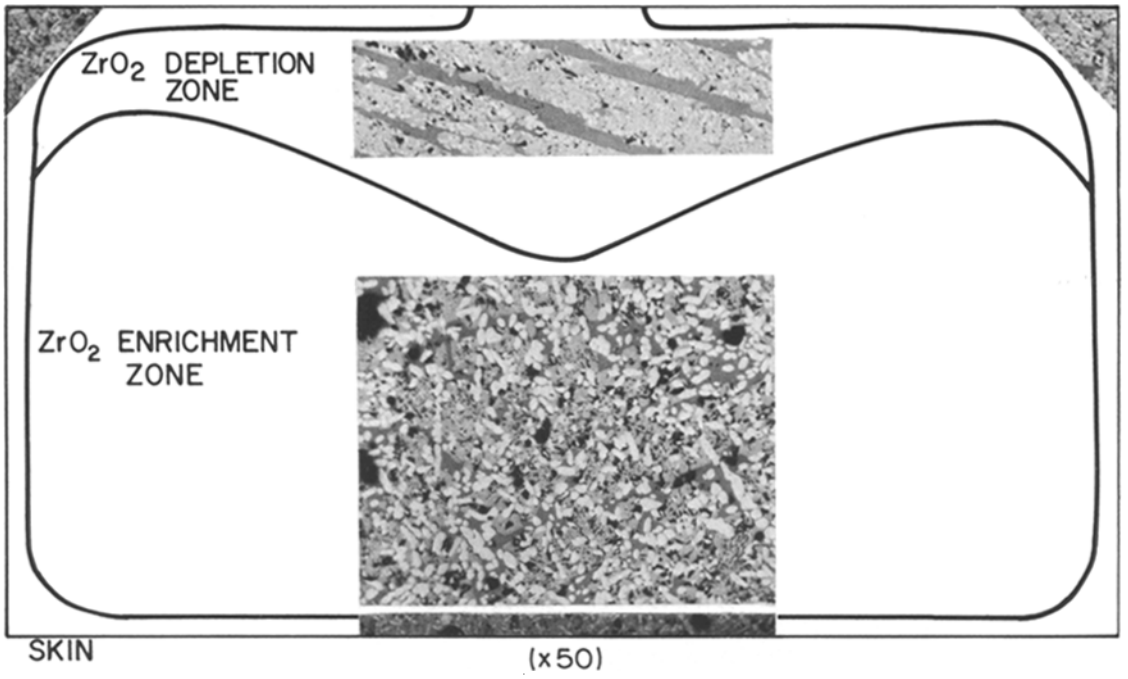

Figure 19 The microstructure at various locations in an Al_2O_3–ZrO_2–SiO_2 fusion-cast refactory.

cracks that make it difficult to handle the casting. Also, the uniformity in the microstructure throughout the volume of a large casting is important to ensure the overall quality of the material. A significant problem that arises during fusion-casting is the differences in composition that occur because of either density differences, convection currents, progressive enrichment of liquid in the lower melting components or interdendritic shrinkage and consequent fluid flow.

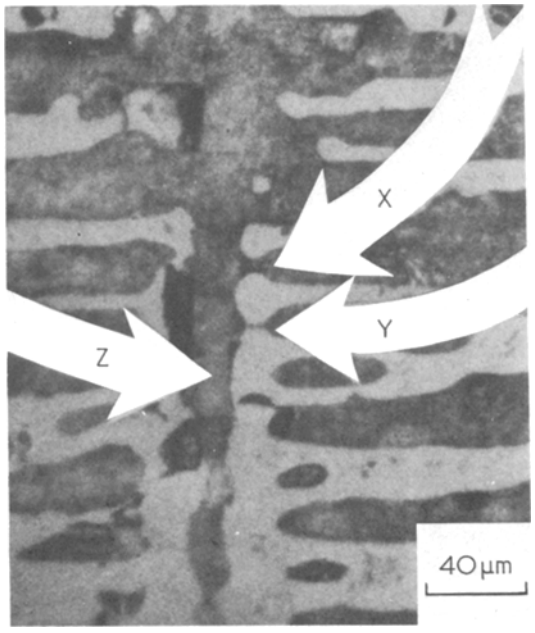

Figure 20 Possible remelting of dendrites in fusion-cast MgO–Al_2O_3 (see text for description).

The effect of density on segregation is shown in Figs. 18 and 19 in the system Al_2O_3–ZrO_2–SiO_2. The material that crystallized near the top of the melt cooled faster and contains mainly α-Al_2O_3 crystals with included ZrO_2 and lies in a glassy matrix. The material at the bottom of the casting, which solidified more slowly, contains much less included ZrO_2 in α-Al_2O_3. These crystals and moderately sized ZrO_2 crystals lie surrounded by the glass. The total concentration of ZrO_2 in the bottom of the casting is significantly higher than that at the top.

In addition to the effect of density, composition segregation results even if equilibrium conditions are followed. Consider, for example, a simple A–B binary eutectic. As the temperature falls below the liquidus in a hypo-eutectic, solidification is initiated with the appearance of crystals of A. As a result, the liquid in which these crystals of A are suspended is enriched in the solute, B. With progressive solidification, the liquid composition travels down the liquidus, getting richer in B until the eutectic is reached. Since the eutectic is an invariant point, the last liquid remaining will (ideally) all freeze at one temperature and at one

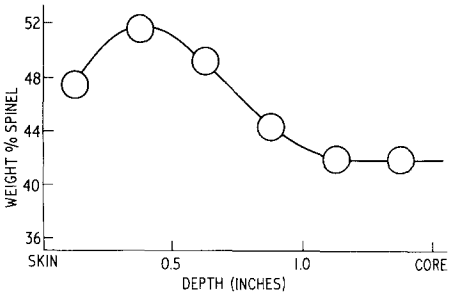

Figure 21 Typical inverse segregation profile in fusion-cast 65 wt% MgO–35 wt% Al_2O_3 refactory ingot.

composition. Since the solidification in a casting progresses from the outer wall (in contact with the mould) to the core of the casting, there is a *normal* segregation that develops in which the interior of the casting is enriched in the lower melting constituents.

Quite a different segregation results because of large interdendritic shrinkage. This is demonstrated best by considering a 65 wt% MgO–35 wt% Al_2O_3 casting where this effect is most pronounced. As mentioned earlier, the outermost skin of a casting being essentially quenched results in a chill zone. Once a thin skin has formed, heat transfer through the insulating layer is not as rapid, but still occurs perpendicular to the frozen wall. Periclase begins to crystallize in dendritic or trellis patterns. The trunks of these dendrites, as shown before, are perpendicular to the chill face. Equilibrium (or slow) cooling conditions cannot develop, primarily because of the considerable volume contraction accompanying the transformation from the liquid to the solid state. The magnitude of this volume contraction is large enough to draw the spinel-enriched residual liquid back along interdendritic channels. This liquid reacts with the early crystallized dendrites forming the rounded grains.* The rounding can also be a result of the remelting of dendrites soon after the crystallization process. Such a remelting process has been hypothesized by Jackson *et al.* [30], and evidence for this is shown in Fig. 20. (At X a neck is seen to be forming at the root of the dendrite arm, at Y the arm is about to detach from the main stem, and at Z the arm is completely detached from the main stem.)

5. Conclusion

Fusion-cast materials are characterized by a microstructure having well-reacted phases, with large interlocking crystals, low porosity and high strength. Fusion casting is a process which has a tendency to produce composition segregation in the ingot and it is difficult to maintain a uniform crystal size.

It should be clear that with the aid of phase diagrams it is possible to predict the type of microstructure that may be obtained with appropriate control over composition, temperature and atmosphere. Other factors which also have to be considered, since they govern both the microstructure and the macrostructure of the cast ingot, are the thermal conductivity, diffusivity, density changes, gas solubility, viscosity and surface tension of the molten and solidified materials.

References

1. E. RUDY, D. P. HARMON and C. E. BRUKL, AFML-TR-65-2 Part IVII, (1966) p. 65.
2. R. N. McNALLY, F. I. PETERS and P. H. RIBBE, *J. Amer. Ceram. Soc.* **44** (1961) 491.
3. R. V. SARA, C. E. LOWELL and R. T. DELLOFF, WADD-TR-60-143 Part IV (1963).
4. R. V. SARA, *J. Amer. Ceram. Soc.* **48** (1965) 243.
5. G. SAMSONOV, N. ZHURAVLEV and J. G. AMNVEL, *Fiz. Metall. Metallov.* **3** (1956) 309.
6. R. T. DOLLOFF, WADD-TR-60-143 July (1960).
7. R. P. ELLIOTT, U.S.E.A.C. Contract No. AT (11-1)-578.
8. J. WHITE, *Refractories J.* **39** (1963) 126.
9. *Idem, Science of Ceramics* **2** (1965) 305.
10. *Idem, J. Aust. Ceram. Soc.* **9** (1973) 26.
11. *Idem, ibid.* **9** (1973) 64.
12. *Idem, ibid.* **10** (1974) 1.
13. B. PHILLIPS and A. MUAN, *J. Phys. Chem.* **64** (1960) 1451.
14. J. C. WILSHEE and J. WHITE, *Trans. Brit. Ceram. Soc.* (1967) 541.
15. L. H. VAN VLACK, *J. Amer. Ceram. Soc.* **43** (1960) 140.
16. L. J. MANFREDO, G. R. FISCHER and R. N. McNALLY, to be published.
17. J. D. HUNT and K. A. JACKSON, *Trans. A.I.M.E.* **236** (1966) 843.
18. K. A. JACKSON, "Mechanism of Growth, Liquid Metals and Solidification" (ASM, Metals Park, Ohio, 1958) p. 174.
19. D. R. UHLMANN, reported by A. M. Alper in "Ceramic Microstructures" edited by R. M. Fulrath and J. A. Pask (John Wiley and Son, New York and London, 1968) p. 763.

*Spinel is thereby concentrated in the content portion of the casting and the periclase crystals are left behind in the core, thus increasing the ratio of the periclase to spinel there. The segregation is the opposite of that normally expected and as such is termed inverse segregation. Typical inverse segregation profiles are shown in Fig. 21. Details of inverse segregation may be found in [31].

20. F. L. KENNARD, R. C. BRADT and U. S. STUBICAN, *J. Amer. Ceram. Soc.* **56** (1973) 566.
21. A. M. ALPER, R. N. McNALLY, P. H. RIBBE and R. C. DOMAN, *ibid.* **45** (1962) 263.
22. A. M. ALPER, R. N. McNALLY, R. C. DOMAN and R. G. KEIHN, *ibid.* **47** (1964) 30.
23. F. MASSAZZA and E. SIRICHIA, *Chim. Ind.* **40** (1958) 378.
24. A. M. ALPER, R. C. DOMAN and R. N. McNALLY, *Science of Ceramics* **4** (1968) 389.
25. E. RUDY, AFML-TR-65-2 Parts IV and V.II (1966).
26. W. J. MINFORD, F. L. KENNARD, R. C. BRADT and V. S. STUBICAN, "Ceramic Microstructures" ed. R. M. Fulrath and J. A. Pask (Westview Press, Boulder, Colorado, 1976) p. 456.
27. R. N. McNALLY and G. H. BEALL, *J. Mater. Sci.* **14** (1979) 2596.
28. A. M. ALPER and R. N. McNALLY, British Patent No. 966,269.
29. R. C. DOMAN, A. M. ALPER and R. N. McNALLY, *J. Mater. Sci.* **3** (1968) 390.
30. K. A. JACKSON, J. D. HUNT, D. R. UHLMANN and T. P. SEWARD, *Trans. A.I.M.E.* **236** (1966) 49.
31. P. H. RIBBE and A. M. ALPER, *J. Amer. Ceram. Soc.* **47** (1964) 162.
32. J. W. WHITE, "High Temperature Oxides, Part I", edited by A. M. Alper (Academic Press, London and New York, 1971).

Received 25 January and accepted 22 February 1980.